

# Wavelet Deconvolution in a Periodic Setting with Long-Range Dependent Errors

Justin Rory Wishart<sup>1</sup>

*Department of Mathematics & Statistics  
The University of Melbourne  
Parkville, VIC, 3010*

---

## Abstract

In this paper, a hard thresholding wavelet estimator is constructed for a deconvolution model in a periodic setting that has long-range dependent noise. The estimation paradigm is based on a maxiset method that attains a near optimal rate of convergence for a variety of  $\mathcal{L}_p$  loss functions and a wide variety of Besov spaces in the presence of strong dependence. The effect of long-range dependence is detrimental to the rate of convergence. The method is implemented using a modification of the `WaveD`-package in R and an extensive numerical study is conducted. The numerical study supplements the theoretical results and compares the LRD estimator with naïvely using the standard `WaveD` approach.

*Keywords:* Besov Spaces, Deconvolution, fractional Brownian motion, Long-Range Dependence, Maxiset theory, Wavelet Analysis

*2010 MSC:* 62G08, 62G05, 62G20

---

## 1. Introduction

Nonparametric estimation of a function in a deconvolution model has been studied widely in various contexts. We study the deconvolution model with a long range dependent (LRD) error structure. More specifically, we consider the problem of estimating a function  $f$  after observing the process,

$$dY(x) = K * f(x) dx + \varepsilon^\alpha dB_H(x), \quad x \in [0, 1]; \quad (1)$$

where  $K * f(x) = \int_0^1 K(t)f(x-t) dt$  is the regular convolution operator,  $\varepsilon \asymp n^{-1/2}$ ,  $B_H$  is a fractional Brownian motion. The fractional Brownian motion is defined as a Gaussian

---

*Email address:* [j.wishart@unsw.edu.au](mailto:j.wishart@unsw.edu.au) (Justin Rory Wishart)

<sup>1</sup>The author has moved since the work was completed. The present address of the author is at the University of New South Wales.

8 process with zero mean and covariance structure,

$$\mathbb{E}B_H(t)B_H(s) = \frac{1}{2} (|s|^{2H} + |t|^{2H} - |t - s|^{2H})$$

9 and  $\alpha = 2 - 2H \in (0, 1]$  is the level of long-range dependence (where  $H$  denotes the standard  
10 Hurst parameter). The assumption of an i.i.d. error structure is captured as a special case  
11 of (1) with the choice  $\alpha = 1$  which reduces the model to a standard Brownian motion  
12 structure. The convolution operator  $K$  is assumed to be of the *regular-smooth* type such  
13 that the Fourier coefficients

$$|\tilde{K}[\omega]| \asymp |\omega|^{-\nu} \quad \text{for all } \omega \in \mathbb{R}, \quad (2)$$

14 where  $\nu \geq 0$  and  $\tilde{K}[\omega]$  denotes the Fourier transform  $\tilde{K}[\omega] = \mathcal{F}K[\omega] := \int_{\mathbb{R}} e^{-2\pi i \omega x} K(x) dx$ .

15 Deconvolution is a common problem occurring in several areas such as econometrics,  
16 biometrics, medical statistics and image reconstruction. For example, the method can be  
17 applied to the light detection and ranging (LIDAR) techniques and image de-blurring tech-  
18 niques. The parameter  $\nu > 0$  is often referred to as the *degree of ill-posedness* (DIP) with  
19  $\nu = 0$  denoting the *well-posed* or direct case.

20 Various wavelet methods have been constructed to address the deconvolution problem  
21 over the last two decades (see for example [Donoho \(1995\)](#); [Wang \(1997\)](#); [Abramovich and Silverman](#)  
22 [\(1998\)](#); [Walter and Shen \(1999\)](#); [Fan and Koo \(2002\)](#); [Donoho and Raimondo \(2004\)](#); [Johnstone and Raimondo](#)  
23 [\(2004\)](#); [Johnstone et al. \(2004\)](#); [Kalifa and Mallat \(2003\)](#); [Pensky and Sapatinas \(2009\)](#)).

24 In the standard deconvolution models, the assumption of i.i.d. variables is made. How-  
25 ever, empirical evidence has shown that even at large lags, the correlation structure in  
26 variables can decay at a hyperbolic rate. To account for this, an extensive literature on LRD  
27 variables has emerged to describe this phenomena. Areas of applications of LRD analysis  
28 include economics with financial returns, volatility and stock trading volumes; hydrology in  
29 rainfall and temperature data; and computer science with data network traffic data. There  
30 are many more applications of LRD analysis and the interested reader is referred to [Beran](#)  
31 [\(1992, 1994\)](#) and [Doukhan et al. \(2003\)](#) for more details. Some analysis has been done for the  
32 direct model ( $\nu = 0$ ) with LRD errors in works such as [Wang \(1996\)](#); [Kulik and Raimondo](#)  
33 [\(2009b\)](#). The topic of density deconvolution with LRD has been studied by [Kulik \(2008\)](#);  
34 [Chesneau \(2012\)](#).

35 The aim of this paper is to study a wavelet deconvolution algorithm that can be easily  
36 applied in the context of a deconvolution problem with LRD errors as in model (1). Minimax

37 rates of estimation of  $f$  have been established in our context by Wang (1997) for the squared-  
 38 error loss. However, their method uses the Wavelet-Vaguelette Decomposition (WVD) which  
 39 is a sophisticated transform where, to the authors knowledge, there is no freely available  
 40 software for implementation.

41 There are two main contributions that this paper will address. The first contribution  
 42 will establish theoretical results for a wide variety of function classes over many error mea-  
 43 sures (which includes the squared-error loss considered in Wang (1997) as a special case) by  
 44 adapting the approaches of Johnstone et al. (2004) and Kulik and Raimondo (2009a). The  
 45 estimation of  $f$  can be achieved with an accuracy of order,

$$\left(\frac{\log n}{n}\right)^\rho, \quad \rho = \frac{\alpha sp}{2s + 2\nu + \alpha},$$

46 where the performance is measured by the error loss from the  $\mathcal{L}_p$  metric. The approach  
 47 of Johnstone et al. (2004) used a hard thresholding wavelet estimator. We modify their  
 48 approach by determining the appropriate threshold levels and fine scale level under the  
 49 strong dependence structure in (1).

50 The second contribution is allowing an easily implementable method for estimation in  
 51 practice by modifying the already established WaveD approach of Raimondo and Stewart  
 52 (2007). The WaveD software is freely available from CRAN (<http://cran.r-project.org/>).  
 53 With our modification of WaveD, a numerical study is conducted comparing the performance  
 54 of the default WaveD method and the LRD method presented here. Four popular test case  
 55 signals are used to benchmark methods in the literature are the Doppler, LIDAR, Bumps  
 56 and Cusp signals. These are used here and are shown in Figure 1.

57 As will become evident in the later in the theoretical analysis. The case of LRD errors  
 58 introduces some challenges to the estimation. For strong dependence there can be artificial  
 59 trends in the noise which require modified thresholds in the wavelet estimator compared to  
 60 the i.i.d. case. These effects are demonstrated clearly in Figure 2 for the cusp signal whereby  
 61 the addition of a higher scale in the wavelet estimation deteriorates the performance of the  
 62 standard WaveD method when there is a strong LRD error structure. Since the finest scale is  
 63 too large, the i.i.d. method also includes the spurious trends which were artificially generated  
 64 by the LRD error sequence.

### 65 1.1. Outline

66 A review of periodised Meyer wavelets and the Besov functional class are given in  
 67 Section 2. In Section 3 the basic argument for the deconvolution technique is given along

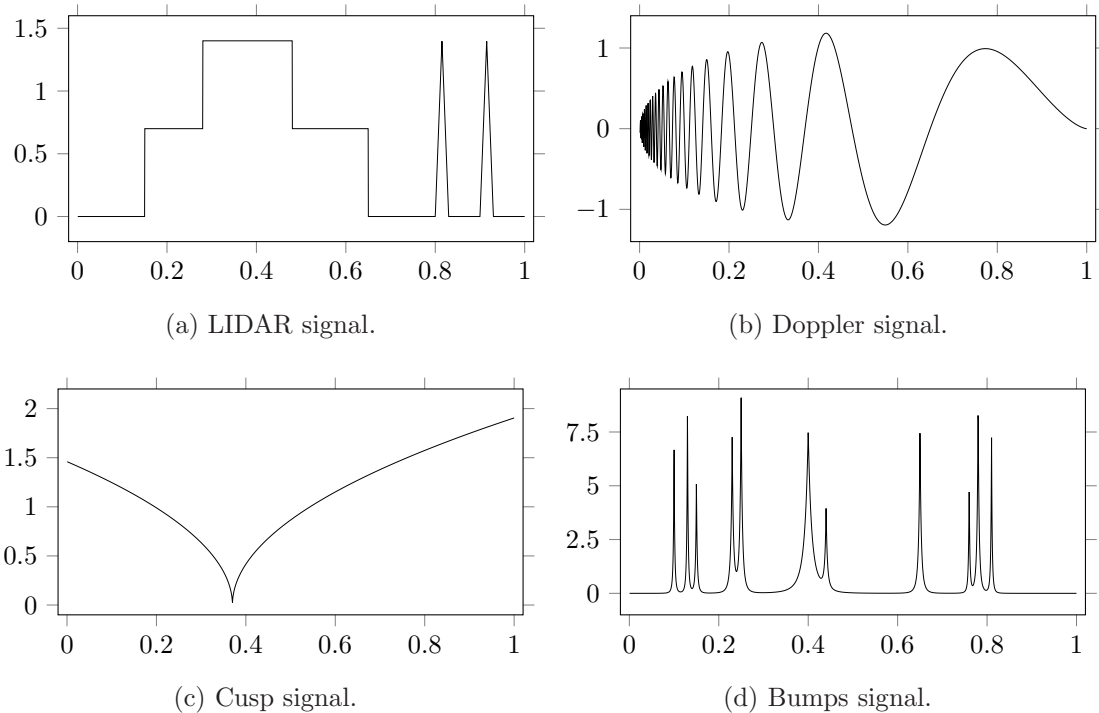


Figure 1: Four signals that are common in signal processing and deconvolution.

68 with the convergence rate results. In [Section 4](#), the method is implemented in R and a nu-  
 69 merical study is conducted to confirm the rate results and a compare with the current WaveD  
 70 methodology. The mathematical proofs are given in [Section 5](#).

## 71 2. Preliminary framework

### 72 2.1. Periodised Meyer wavelet basis

73 Let  $(\phi, \psi)$  denote the Meyer wavelet scaling and detail basis functions defined on the real  
 74 line  $\mathbb{R}$ ; (see [Meyer \(1992\)](#) and [Mallat \(1999\)](#)). These are defined in the Fourier domain with,

$$\tilde{\phi}(\omega) = \begin{cases} 1, & \text{if } |\omega| \leq 1/3 \\ \cos(\pi/2v(3|\omega| - 1)), & \text{if } |\omega| \in (1/3, 2/3] \\ 0, & \text{otherwise.} \end{cases}$$

75 and the mother wavelet function defined with,

$$\tilde{\psi}(\omega) = \begin{cases} e^{-i\pi\omega} \sin(\frac{\pi}{2}v(3|\omega| - 1)), & \text{if } |\omega| \in (1/3, 2/3] \\ e^{-i\pi\omega} \cos(\frac{\pi}{2}v(3/2|\omega| - 1)), & \text{if } |\omega| \in (2/3, 4/3] \\ 0, & \text{otherwise.} \end{cases} \quad (3)$$

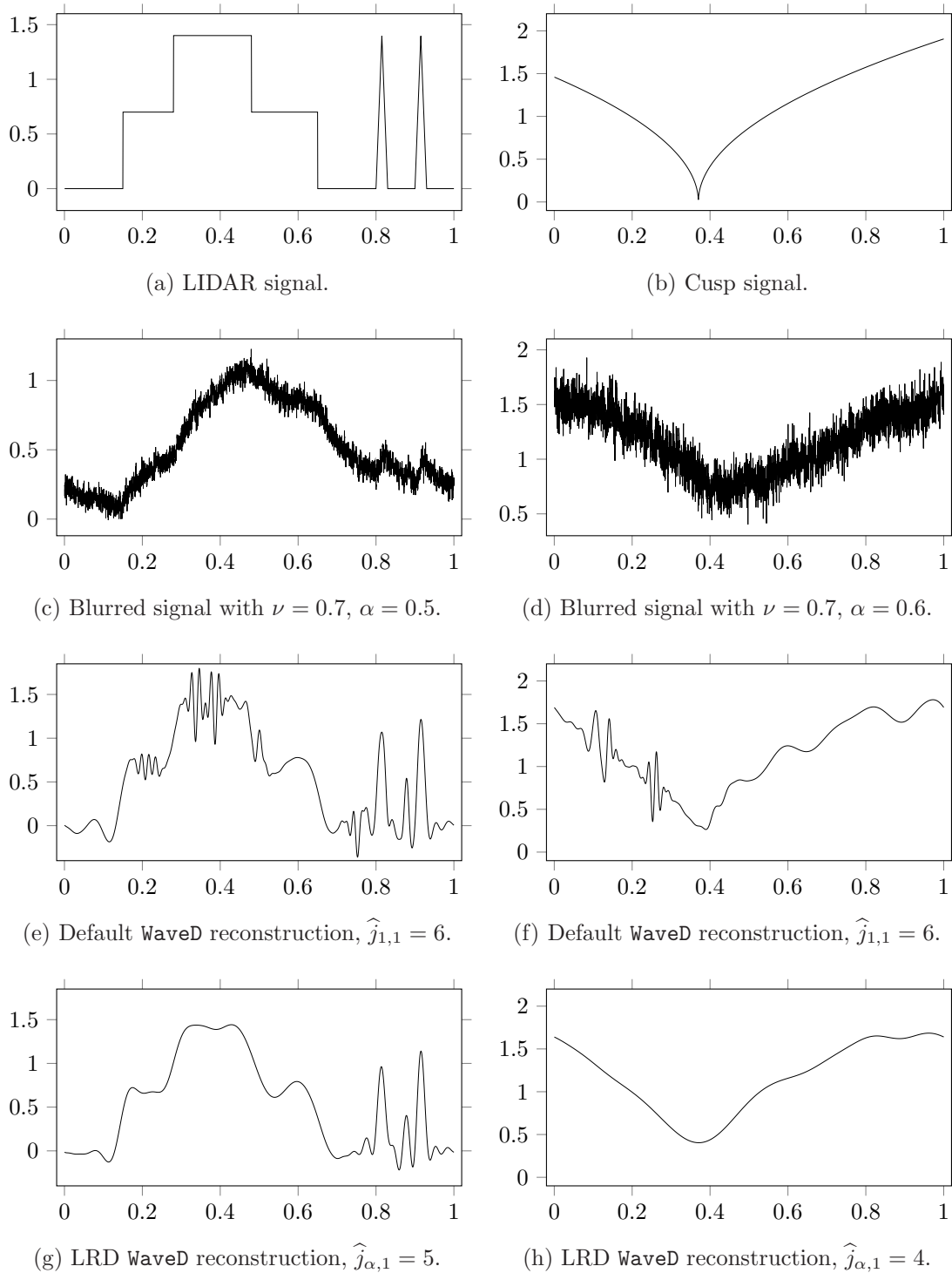


Figure 2: Comparison of the LRD WaveD method against the default WaveD method. In both cases,  $n = 4096 = 2^{12}$ . The LRD method truncates the finest scale earlier as noted. For the LIDAR and cusp signals,  $\text{SNR} \approx 20\text{dB}$ .

76 The auxiliary function  $v$  is a piecewise polynomial that can be chosen to ensure that the  
77 Meyer wavelet has enough vanishing moments. For the bivariate index  $(j, k)$ , the dilated and

78 translated mother and father wavelets at resolution level  $j$  and time position  $k$  are defined,

$$\phi_{j,k}(x) = 2^{j/2}\phi(2^j x - k), \quad \psi_{j,k}(x) = 2^{j/2}\psi(2^j x - k), \quad \text{for } j \geq 0.$$

79 For our purposes, we are interested with a multiresolution analysis for periodic functions on  
80  $\mathcal{L}_2([0, 1])$ . This is done by periodising the Meyer basis functions with,

$$\Phi_{j,k}(x) = \sum_{l \in \mathbb{Z}} \phi_{j,k}(x + l) \quad \text{and} \quad \Psi_{j,k}(x) = \sum_{l \in \mathbb{Z}} \psi_{j,k}(x + l).$$

81 Consequently, any 1-periodic function  $f \in \mathcal{L}_2([0, 1])$  can be written with a wavlet expansion  
82 with,

$$f(x) = \sum_{k=j_0}^{2^{j_0}-1} \alpha_{j_0,k} \Phi_{j_0,k}(x) + \sum_{j=j_0}^{\infty} \sum_{k=0}^{2^j-1} \beta_{j,k} \Psi_{j,k}(x),$$

83 where  $\alpha_{j_0,k} = \langle f, \Phi_{j_0,k} \rangle = \int_0^1 f(t) \Phi_{j_0,k}(t) dt$  and  $\beta_{j,k} = \langle f, \Psi_{j,k} \rangle = \int_0^1 f(t) \Psi_{j,k}(t) dt$ .

84 This particular expansion is used since the Meyer wavelet is bandlimited (see (3)) which  
85 allows the use of efficient algorithms with [Raimondo and Stewart \(2007\)](#) and for mathemat-  
86 ical convenience in the later proofs.

## 87 2.2. Functional Class

88 We analyse the estimation procedure over a Besov space of periodic functions which have  
89 a nice characterisation using the coefficients of a wavelet expansion (granted that the wavelet  
90 is periodic and has enough smoothness and vanishing moments).

91 **Definition 1.** For  $f \in \mathcal{L}_\pi([0, 1])$  with  $\pi \geq 1$  and  $r \geq 1$ ,

$$f = \sum_{j,k} \beta_{j,k} \Psi_{j,k}(x) \in \mathcal{B}_{\pi,r}^s \Leftrightarrow \sum_{j \geq 0} 2^{j(s + \frac{1}{2} - \frac{1}{\pi})r} \left( \sum_{k=0}^{2^j} |\beta_{j,k}|^\pi \right)^{\frac{r}{\pi}} < \infty.$$

92 The consideration of a Besov class allows a more precise analysis of the asymptotic conver-  
93 gence results of the signal  $f$  since the Besov class includes other common functional classes  
94 as a special case. Loosely speaking, a function  $f \in \mathcal{B}_{\pi,r}^s$  includes functions that are  $s$  times  
95 differentiable with  $f^{(s)} \in \mathcal{L}_\pi(0, 1)$ . The parameter  $r$  is less important, it allows a more  
96 intricate variation of behaviour in the Besov class. The special cases when  $\pi$  or  $r = \infty$   
97 involve replacing the  $\ell_\pi$  and  $\ell_r$  type norms in [Definition 1](#) with the  $\ell_\infty$  norm. For exam-  
98 ple, if  $f \in \mathcal{B}_{\infty,\infty}^s \Rightarrow \sup_{j \geq 0} 2^{j(s+1/2-1/\pi)} \sup_{(j,k)} |\beta_{j,k}| < \infty$ . The interested reader is referred  
99 to [Donoho et al. \(1995\)](#); [Donoho and Johnstone \(1998\)](#) and references therein for a more  
100 detailed discussion.

### 101 3. Function estimation method

102 We use the wavelet shrinkage paradigm for our estimation which has become a standard  
 103 statistical procedure in nonparametric estimation. We use a hard thresholding approach  
 104 where the wavelet estimator is defined,

$$\widehat{f}(x) = \sum_{k=0}^{2^{j_0}-1} \widehat{\alpha}_{j_0,k} \mathbb{1}_{\{|\widehat{\alpha}_{j_0,k}| \geq \lambda_{j_0}\}} \Phi_{j_0,k}(x) + \sum_{(j,k) \in \Lambda_n} \widehat{\beta}_{j,k} \Psi_{j,k}(x), \quad (4)$$

105 where  $\widehat{\alpha}_{j_0,k}$  and  $\widehat{\beta}_{j_0,k}$  are the estimated wavelet coefficients. The level  $j_0$  corresponds to the  
 106 coarse resolution level and the set of indices  $\Lambda_n = \{(j, k) : j_0 \leq j \leq j_1; k = 0, 1, \dots, 2^j - 1\}$   
 107 indexes details of the function up to a fine resolution level  $j_1$ . The wavelet estimation  
 108 procedure keeps only the coefficients in the expansion when  $|\widehat{\beta}_{j,k}| \geq \lambda_j$ , a scale dependent  
 109 threshold. The parameters  $\lambda_j$  and indices  $\Lambda_n$  are chosen to control the noise embedded in  
 110 the estimated wavelet coefficients in an optimal way in the sense of the rate results presented  
 111 in the next section.

112 For the deconvolution problem it is natural to conduct analysis in the Fourier domain  
 113 since the deconvolution operator becomes a multiplier in the Fourier domain. The deconvolution  
 114 model, (1), has Fourier domain representation with,

$$\widetilde{Y}[n] := \int_{\mathbb{R}} e^{-2\pi i n x} dY(x) = \widetilde{K}[n] \widetilde{f}[n] + \varepsilon^\alpha \widetilde{Z}_H[n].$$

Then using the Parseval identity, one can obtain a representation of the wavelet coefficients.

$$\begin{aligned} \widehat{\beta}_{j,k} &= \sum_{n \in \mathbb{Z}} \frac{\widetilde{Y}[n]}{\widetilde{K}[n]} \overline{\Psi_{j,k}[n]} \\ &= \sum_{n \in \mathbb{Z}} \widetilde{f}[n] \overline{\Psi_{j,k}[n]} + \varepsilon^\alpha \sum_{n \in \mathbb{Z}} \frac{\widetilde{Z}_H[n]}{\widetilde{K}[n]} \overline{\Psi_{j,k}[n]} \\ &= \beta_{j,k} + \varepsilon^\alpha \sum_{n \in \mathbb{Z}} \frac{\widetilde{Z}_H[n]}{\widetilde{K}[n]} \overline{\Psi_{j,k}[n]} \end{aligned} \quad (5)$$

115 The Meyer wavelet is bandlimited (see (3)) meaning that the sums are finite. In particular,  
 116 define the summation sets for the detail coefficients at scale level  $j$  with,

$$\mathbb{D}_j := \{z = \pm a : a \in \{[2^j/3], [2^j/3] + 1, \dots, [2^{j+2}/3]\}\}, \quad (6)$$

117 which has cardinality  $|\mathbb{D}_j| = 2^{j+1}$ . A similar procedure is conducted to estimate the scale  
 118 coefficients  $\alpha_{j_0,k}$  by using the Fourier coefficients of the scale function  $\Phi_{j_0,k}$  instead of the  
 119 detail function  $\Psi_{j,k}$ .

120 *3.1. Maxiset Approach*

121 The methodology used here is an amalgamation of the deconvolution work of [Johnstone et al.](#)  
 122 (2004) and the LRD work of [Kulik and Raimondo \(2009b\)](#). The nonlinear wavelet estimator  
 123 (4) can be analysed using the maxiset approach with the level dependent threshold  $\lambda = \lambda_j$   
 124 and fine resolution level  $j_1$  which depends on  $\alpha$  and  $\nu$ .

125 *Fine resolution level.* The range of resolution levels (frequencies) where the estimator (4)  
 126 is considered is,

$$\Lambda_n = \{(j, k) : j_0 \leq j \leq j_1, 0 \leq k \leq 2^j\}. \quad (7)$$

127 The finest resolution level  $j_1$  is set to be,

$$2^{j_1} = 2^{j_{\alpha,1}} := \left( \frac{n^\alpha}{\log n} \right)^{1/(\alpha+2\nu)}, \quad (8)$$

128 Then consider the precise form of the level dependent thresholds in  $\lambda = \lambda_j$ . As in previous  
 129 works, this level dependent threshold will have three input parameters, written,

$$\lambda_j = \xi \sigma_{j,\nu,\alpha} c_n, \quad (9)$$

130 where the three values are given by,

- 131 •  $\xi$  : a constant that depends on the tail of the noise distribution. Theoretically this  
 132 should satisfy the bound  $\xi > 2\sqrt{\alpha(p \vee 2)}$ .
- 133 •  $\sigma_j$ : the level-dependent scaling factor that is based on the convolution kernel and level  
 134 of dependence,

$$\sigma_j = \sigma_{j,\nu,\alpha} = \mathcal{O}(2^{-j(1-\alpha-2\nu)/2}). \quad (10)$$

- 135 •  $c_n$  : a sample size dependent scaling factor,

$$c_n = \sqrt{n^{-\alpha} \log n}. \quad (11)$$

136 The smoothing parameter is intentionally denoted  $\xi$  to distinguish it clearly from the smooth-  
 137 ing parameter, denoted  $\eta$  used in the i.i.d. case in [Johnstone et al. \(2004\)](#) and its WaveD  
 138 implementation in [Raimondo and Stewart \(2007\)](#).

139 **Theorem 1.** Consider model (1) with the wavelet estimator (4) with the coefficient esti-  
 140 mates in (5) using the thresholds and resolution levels given by, (7), (8), (9), (10) and (11).

141 Assume that  $p > 1$  and  $f \in \mathcal{B}_{\pi,r}^s$  with  $\pi \geq 1$ ,  $s \geq 1/\pi$  where  $r$  satisfies

$$0 < r \leq \min \left\{ \frac{(2\nu + \alpha)p}{2s + 2\nu + \alpha}, \frac{(2\nu + \alpha)p - 2}{2s + 2\nu - \frac{2}{\pi}\alpha} \right\}.$$



142 Then there exists a constant  $C > 0$  such that,

$$\mathbb{E} \left\| f - \hat{f} \right\|_p^p \leq C \left( \frac{\log n}{n} \right)^\rho,$$

where  $\|\cdot\|_p$  is the standard  $p$ -norm and,

$$\rho = \begin{cases} \frac{\alpha sp}{2s + 2\nu + \alpha}, & \text{if } s \geq (2\nu + \alpha) \left( \frac{p}{2\pi} - \frac{1}{2} \right); \\ \frac{\alpha p (s - \frac{1}{\pi} + \frac{1}{p})}{2s + 2\nu + \alpha - \frac{2}{\pi}}, & \text{if } \frac{1}{\pi} - \nu - \frac{\alpha}{2} < s < (2\nu + \alpha) \left( \frac{p}{2\pi} - \frac{1}{2} \right). \end{cases} \quad (12)$$

143 **Remark 1.** There is an ‘elbow effect’ or ‘phase transition’ in the rates of convergence switch-  
 144 ing from (12) to (13) which are usually referred to as the ‘dense’ and ‘sparse’ phases respec-  
 145 tively. This is similar to the effect seen in [Kulik and Raimondo \(2009a\)](#) and [Johnstone et al.](#)  
 146 [\(2004\)](#). The fBm errors has increased the size of the dense region in comparison to the stan-  
 147 dard Brownian motion when the boundary was at  $s = (2\nu + 1)(p/2\pi - 1/2)$  (see [Johnstone et al.](#)  
 148 [\(2004\)](#)). Also for the sparse region, the condition  $p > 2/(2\nu + \alpha)$  is needed to ensure that it  
 149 is well defined. When  $2\nu + \alpha \geq 2$ , this is not a restriction since it is assumed that  $p > 1$ .

150 **Remark 2.** The rate results are consistent with works on LRD and inverse problems in  
 151 the literature in the sense that the rate of convergence deteriorates as  $\alpha$  decreases (stronger  
 152 dependence) or the DIP parameter  $\nu$  increases (more ill-posed). In particular, our rate results  
 153 agree with the results obtained in [Johnstone et al. \(2004\)](#) in the i.i.d. deconvolution setting  
 154 with smooth convolution,  $|\tilde{K}(\omega)| \sim |\omega|^{-\nu}$ , with the choice  $\alpha = 1$ . Our rate results also agree  
 155 with the results obtained in [Kulik and Raimondo \(2009a\)](#) with the direct regression model  
 156 with LRD errors with the choice  $\nu = 0$ . The results agree with minimax results the for the  
 157 squared-error loss ( $p = 2$ ) by [Wang \(1997\)](#).

158 **Remark 3.** Our estimator is adaptive with respect to the smoothness parameter  $s$  since the  
 159 tuning paradigm does not depend on  $s$ . However it is not adaptive with respect to the LRD  
 160 parameter  $\alpha$  since the level dependent thresholds, (8), (10) and (11) depend on  $\alpha$ .

## 161 4. Numerical Study

162 A numerical study is now considered with the focus being the effect of the dependence  
 163 structure. Ideally, it would be desirable to compare the LRD WaveD method introduced  
 164 here with the minimax optimal WVD method considered by [Wang \(1997\)](#). However, to the  
 165 authors knowledge, no freely available implementation of the WVD method exists.

166 One of the immediate challenges of implementing the LRD approach is that  $\alpha$  is unknown  
 167 in practice. The estimation of  $\alpha$  is a challenging problem in its own right that has been studied  
 168 in the literature, see for example [Veitch and Abry \(1999\)](#) and more recently [Park and Park](#)  
 169 [\(2009\)](#) in this regard. Having full data driven estimates of all the parameters is beyond the  
 170 scope of this work and we will assume that  $\alpha$  is known. For our purposes we wish to compare  
 171 the performance of the regular WaveD approach which was designed for i.i.d. observations  
 172 with the LRD extension suggested here.

173 The default WaveD method uses a stopping rule in the Fourier domain using the results of  
 174 [Cavalier and Raimondo \(2007\)](#) to estimate the finest permissible scale level in the expansion.  
 175 This concerns the case of model (1) with a standard Brownian motion ( $\alpha = 1$ ) where  
 176  $2^{j_1} = 2^{j_{1,1}} = (n/\log n)^{1/(1+2\nu)}$ . For a fair comparison, the finest permissible scale level,  $j_{\alpha,1}$ ,  
 177 should be estimated in the same vein for our LRD extension. The Fourier stopping rule is  
 178 extended to the LRD framework below.

179 Briefly reviewing the fine scale estimation method of [Cavalier and Raimondo \(2007\)](#), the  
 180 scenario of an unknown convolution kernel  $K$  is considered. To alleviate this they assume  
 181 that it is possible to choose input signals  $f$  in (1) to gain information about  $K$ . In particular,  
 182 the Fourier basis is chosen  $f = (e_\ell)_{\ell \in \mathbb{Z}}$  and passed into the deconvolution model. Doing  
 183 so here, one would pass the Fourier basis into (1) and denote this new information with  
 184  $dY_e(x) = K * e_\ell(x) + \varepsilon^\alpha dB_H(x)$ . Due to the orthogonality of the Fourier basis, the Fourier  
 185 domain representation of  $Y_e$  is

$$\tilde{Y}_e[\ell] = \tilde{K}[\ell] + \varepsilon^\alpha W_H[\ell]$$

186 where  $\tilde{W}_H[\ell]$  is a complex Gaussian random variable identically distributed to  $\tilde{Z}_H[\ell]$  but  
 187 independent of  $\tilde{Z}_H[\ell]$ . We then estimate the fine scale level by,

$$\hat{j}_{\alpha,1} = \lfloor \log_2 M \rfloor - 1 \tag{14}$$

188 where the stopping time  $M$  is determined in the Fourier domain with,

$$M = \min \left\{ \ell, \ell > 0 : |\tilde{Y}_e[\ell]| \leq \ell^{\alpha/2} \varepsilon^\alpha \log 1/\varepsilon^2 \right\},$$

189 and  $\lfloor x \rfloor$  is the largest integer small than  $x$ . The estimate  $\hat{j}_{\alpha,1}$  is close to  $j_{\alpha,1}$  with high  
 190 probability due to [Lemma 1](#) in [Section 5](#).

#### 191 4.1. Implementation procedure

192 We are now in a position to be able to implement an estimation procedure for the LRD  
 193 model (1) using a modification of WaveD method of [Raimondo and Stewart \(2007\)](#). This is

194 conducted using the test functions shown in [Figure 1](#). A discretely sampled deconvolution  
 195 model is repeatedly simulated with these test signals and the `WaveD` and LRD modification  
 196 estimates computed. The performance measure is the Mean-Square Error (MSE) which is  
 197 calculated empirically over  $M = 1024$  repeated simulations.

- 198 1. Choose  $f(t)$  to be a LIDAR, Doppler, Bumps or Cusp signal (see [Figure 1](#)) over the  
 199 grid  $t_i = i/n$  with  $i = 1, 2, \dots, n$  and  $n = 2^{12} = 4096$ . The LIDAR and Doppler signals  
 200 were generated from by the code from the `WaveD` package and the Bumps and Cusp  
 201 signal code was imported into R from the `WaveLab` package in MATLAB. The signals were  
 202 standardised to agree with the signal levels in [Cavalier and Raimondo \(2007\)](#).
- 203 2. Simulate the LRD error process using the `fracdiff` package of R available from CRAN.  
 204 Use the `fracdiff.sim` command to simulate a FARIMA sequence, the parameters  
 205 kept at their defaults with the dependence controlled with  $d = (1 - \alpha)/2$  and the LRD  
 206 error process was standardised to have unit variance.
- 207 3. Generate the convolution kernel,  $K = k$ , to be the Gamma density with scale parameter  
 208 0.25 and shape parameter 0.7 (The *DIP* in this case is  $\nu = 0.7$ ).
- 209 4. Generate the data  $y_i = k * f(t_i) + \sigma 2^{-\alpha/2} e_i$  where  $e_i$  is the FARIMA sequence. The  
 210 size of  $\sigma$  is governed by the blurred signal-to-noise ratio (SNR) where

$$\text{SNR} = 10 \log_{10} (\|K * f\|^2 / \sigma^2)$$

211 The SNR is considered for three scenarios SNR = 10dB (high noise), 20dB (medium  
 212 noise) or 30dB (low noise).

- 213 5. Compute the default `WaveD` estimator which assumes three vanishing moments and  
 214 starts the wavelet expansion at scale level  $j_0 = 3$ . The level dependent thresholds are  
 215 computed,  $\lambda_j = \eta \tau_j c_n$  where  $\eta = \sqrt{6}$ ,  $c_n = \hat{\sigma} \sqrt{\log n/n}$  and  $\tau_j = (|\mathbb{D}_j|^{-1} \sum_{\mathbb{D}_j} |K[\ell]|^{-2})^{-1/2}$ .  
 216 The estimated noise level,  $\hat{\sigma} = MAD(y_{J,k})/0.6745$  where  $MAD$  is the median abso-  
 217 lute deviations and  $y_{J,k} = \langle y, \Psi_{J,k} \rangle$ , the wavelet coefficients at the finest scale. The  
 218 fine scale  $j_1 = j_{1,1}$  is estimated using the default `WaveD` method which is based on  
 219 [Cavalier and Raimondo \(2007\)](#).
- 220 6. Compute the LRD `WaveD` estimator which uses the same hard thresholding wavelet  
 221 expansion. However, now the fine scale level and level dependent thresholds are mod-  
 222 ified. The fine scale level,  $j_1 = j_{\alpha,1}$  is estimated using (14) and the level dependent  
 223 thresholds are estimated using  $\hat{\lambda}_j = \xi \tau_{\alpha,j} c_n$  where  $c_n = \hat{\sigma} \sqrt{\log n/n^\alpha}$  and  $\tau_{\alpha,j}$  calculated  
 224 using (31) and (33). The smoothing parameter  $\xi$  was tested for various different values.

225 Similar to the i.i.d. case seen in [Johnstone et al. \(2004\)](#), the default bound given in  
 226 the theory with  $\xi \geq 2\sqrt{2\alpha}$  was much too conservative. Instead the performance was  
 227 found to be much better with the choice  $\xi = \sqrt{\alpha}$ . The presented results here are for  
 228 the choices  $\xi = \sqrt{\alpha}$  and  $\xi = \sqrt{2\alpha}$ , the latter being more effective with low levels of  
 229  $\alpha$ . In fact, the simulations were also conducted for  $\xi = \sqrt{4\alpha}, \sqrt{6\alpha}$  and  $\sqrt{8\alpha}$ . These  
 230 bigger smoothing parameters were only competitive for the cases when  $\alpha \leq 0.3$  and  
 231 are omitted from the tables for brevity.

232 7. Compute the empirical version of the MSE where,

$$\widehat{MSE}(\hat{f}, f) = \widehat{\mathbb{E}} \left\| \hat{f} - f \right\|_2^2 = \frac{1}{M} \sum_{i=1}^M \left\| \hat{f}_i - f \right\|_2^2.$$

#### 233 4.2. Numerical results

234 The results of the procedure are outlined in [Table 1](#) and [Table 2](#). As stated earlier, the  
 235 focus of the numerical study is the effect of the dependence structure so the DIP is fixed at  
 236  $\nu = 0.7$ . The most obvious fact is that overall the convergence rate tends to deteriorate as  
 237 the level of dependence increases. This is consistent with the theoretical results in [Section 3](#).

238 The numerical results are not overall conclusive in favour of one method over the other for  
 239 all noise levels. The main complication arises in the truncation of the wavelet expansion with  
 240 the fine scale levels  $\hat{j}_1$  and  $\hat{j}_{\alpha,1}$ . The typical fine scale levels (rounded to the nearest integer)  
 241 are shown in [Table 1](#) and [Table 2](#) stated in parentheses for each case for each method. Due  
 242 to the construction,  $j_{\alpha,1} \leq j_{1,1}$  for all  $\alpha \in (0, 1]$  and this is reflected in their estimates shown  
 243 in [Table 1](#) and [Table 2](#). As expected  $\hat{j}_{\alpha,1}$  decreases as  $\alpha$  increases (stronger dependence)  
 244 which is consistent with the theory. On the other hand, the naïve i.i.d. estimator increases  
 245 as  $\alpha$  decreases which can be either detrimental or beneficial to estimation as discussed below.

246 In some cases the earlier truncation in the LRD method is favourable such as the LIDAR  
 247 and Cusp signals with a strong level of dependence which is shown in [Figure 2](#). The addition  
 248 of higher scales to the wavelet expansion in the i.i.d. method does contribute to capturing  
 249 more of the cusp feature and the last two peaks of the LIDAR signal. However, it is paid  
 250 at the price that higher scales include spurious effects from the LRD noise, resulting in a  
 251 poor estimator. This is reflected in [Table 1](#) where the MSE is smaller when  $\hat{j}_{\alpha,1} < \hat{j}_1$  with  
 252 the exception at the LIDAR signal at 20dB and  $\alpha = 0.6$  and the Cusp signal at 10dB and  
 253  $\alpha = 0.8$ .

254 On the other hand, the earlier truncation of fine scale levels in the LRD method means  
 255 that important features are not captured in the signal. This is seen in the Bumps and

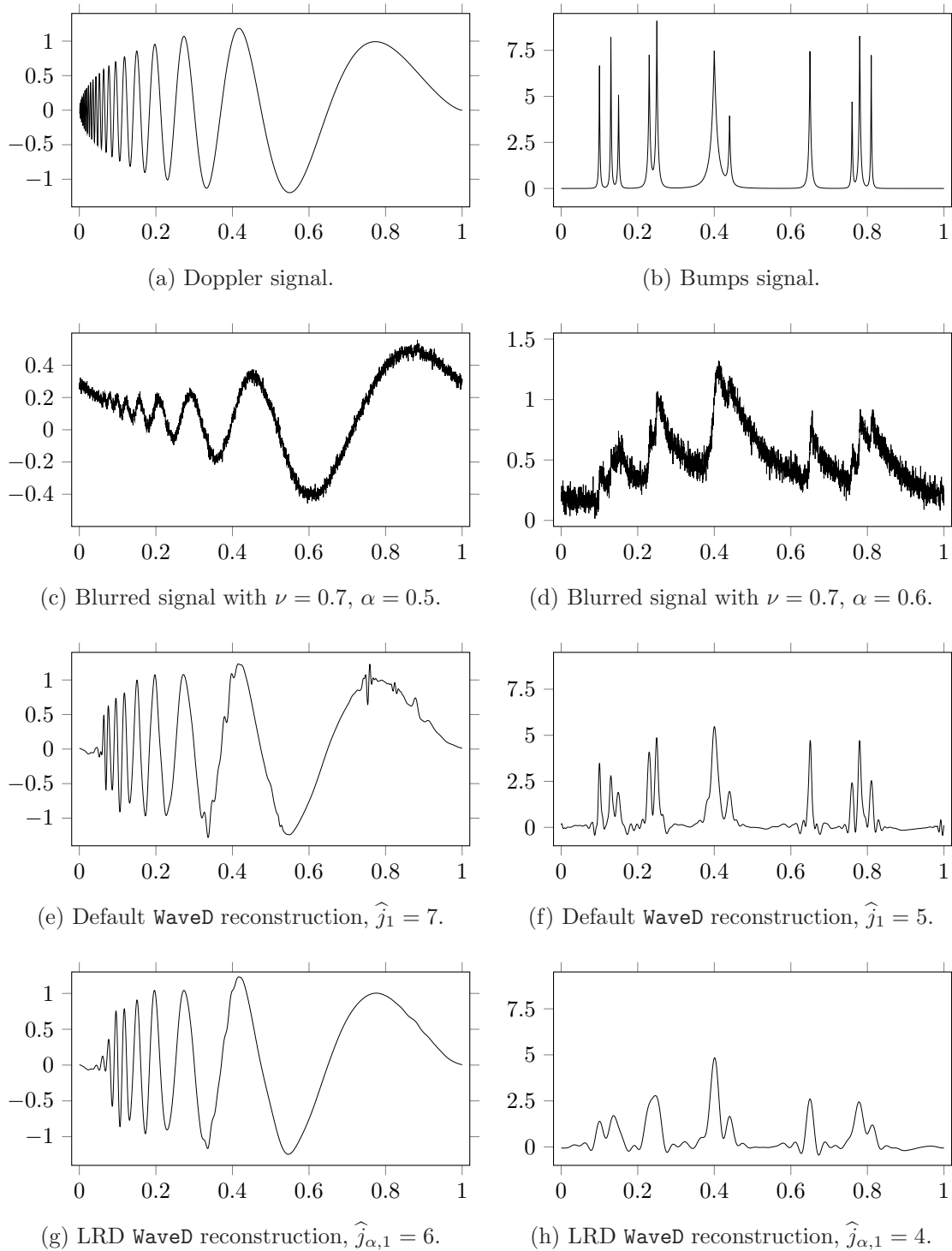


Figure 3: Comparison of the LRD WaveD method against the default WaveD method. In both cases,  $n = 4096 = 2^{12}$ . The LRD method truncates the finest scale earlier as noted. For the Bumps and Doppler signals,  $\text{SNR} \approx 20\text{dB}$ .

256 Doppler signals where the i.i.d. method tends to outperform the LRD method. In this  
 257 situation the higher level scales in the expansion capture more features in the signal while not  
 258 introducing the too much of the spurious LRD noise effects. A typical medium noise scenario

259 demonstrating this is shown for the Bumps and Doppler signals in [Figure 3](#). Referring to  
260 the Doppler deconvolution in [Figure 3](#) one can see that the spurious trends generated by  
261 the LRD noise are included in the default `WaveD` reconstruction, however since  $\hat{j}_1 > \hat{j}_{\alpha,1}$ ,  
262 the higher frequencies of the Doppler signal can be captured. The LRD method does not  
263 include the spurious trends but pays the price of losing the higher frequencies in the Doppler  
264 signal. A similar behaviour is present in the Bumps signal. This behaviour is reflected in  
265 the numerical study in [Table 2](#) where the earlier truncation shows that the i.i.d. method  
266 outperforms the LRD method. However for the case of severely dependent noise at  $\alpha = 0.2$   
267 for the Doppler signal, the i.i.d. method loses its advantage and the addition of higher scales  
268 does not outperform the LRD method.

269 Therefore the LRD estimation method presented here offers an easily implementable so-  
270 lution that is resistant to the effects of long memory. The method is attractive to the case  
271 where the underlying function  $f$  does not have a lot of transient high frequency behaviours  
272 where the higher scales of the wavelet transform are crucial. In the case where high frequen-  
273 cies are crucial to the signal, the established i.i.d. `WaveD` method is perhaps more favourable  
274 since the signal features at higher scales are more important than the spurious noise.

## 275 5. Proofs

First the probabilistic result of the numerical estimation of the highest permissible scale level is given. Define the frequency levels,

$$M_c = \min \left\{ \ell, \ell > 0 : |\tilde{K}[\ell]| \leq \ell^{\alpha/2} \varepsilon^\alpha (\log 1/\varepsilon^2)^{4/3} \right\} \quad (15)$$

$$M_d = \min \left\{ \ell, \ell > 0 : |\tilde{K}[\ell]| \leq \ell^{\alpha/2} \varepsilon^\alpha (\log 1/\varepsilon^2)^{2/3} \right\}. \quad (16)$$

276 **Lemma 1.** *Define the event,  $\mathcal{B} = \bigcap_{\omega=1}^{M_d} \left\{ |\varepsilon^\alpha \tilde{Z}_H[\omega]| \leq |\tilde{K}[\omega]|/2 \right\}$ . Then*

$$P(\mathcal{B}^c) \leq c M_d \exp \left\{ -(\log 1/\varepsilon)^{1+\xi} \right\} =: \Omega_n$$

277 *for some constants  $c, \xi > 0$ . Further, define the event,  $\mathcal{M} = \{M_c \leq M \leq M_d\}$  then  $P(\mathcal{M}^c) =$   
278  $\mathcal{O}(\Omega_n)$  and  $M_c \leq M_d \leq M_1$  where  $M_1 = \lfloor 2^{j_1} \rfloor$ .*

PROOF OF [LEMMA 1](#). First we prove the statement that,  $P(\mathcal{B}^c) \leq \Omega_n$ . By definition of  $M_d$  in [\(16\)](#) there exists a  $c \in (0, 1)$  such that for all  $\omega = 1, 2, \dots, M_d$ ;  $|\tilde{K}[\omega]|/2 >$

$\frac{c}{2}\ell^{\alpha/2}\varepsilon^\alpha (\log 1/\varepsilon)^{2/3}$ . Thus,

$$\begin{aligned} P(\mathcal{B}^c) &= P\left(\bigcup_{\omega=1}^{M_d} \left\{ |\varepsilon^\alpha \tilde{Z}_H[\omega]| > \frac{|\tilde{K}[\omega]|}{2} \right\}\right) \\ &\leq \sum_{\omega=1}^{M_d} P\left(|\varepsilon^\alpha \tilde{Z}_H[\omega]| > |\tilde{K}[\omega]|/2\right) \\ &\leq \sum_{\omega=1}^{M_d} P\left(|\tilde{Z}_H[\omega]| > \frac{c}{2}\omega^{\alpha/2} (\log 1/\varepsilon^2)^{2/3}\right) \end{aligned}$$

From (32),  $\text{Var}\left(\tilde{Z}_H[\omega]\right) \asymp |\omega|^{\alpha-1}$  and apply the tail inequality for Gaussian random variables, let  $Z \sim \mathcal{N}(0, 1)$ , then there exists a constant  $C > 0$  such that,

$$\begin{aligned} P(\mathcal{B}^c) &\leq \sum_{\omega=1}^{M_d} P\left(|Z| > c\omega^{1/2} (\log 1/\varepsilon^2)^{2/3}\right) \\ &\leq CM_d \exp\left\{-\frac{1}{2}c^2 (\log 1/\varepsilon)^{4/3}\right\} = \mathcal{O}(\Omega_n). \end{aligned} \quad (17)$$

For  $\mathcal{M}^c$  the event can be written  $\mathcal{M}^c = \{M > M_d\} \cup \{M < M_c\}$  and start by considering the first scenario,

$$\begin{aligned} P(M > M_d) &\leq P\left(\bigcap_{\omega=1}^{M_d} \left\{ |\tilde{Y}_e[\omega]| > \omega^{\alpha/2} \varepsilon^\alpha \log 1/\varepsilon^2 \right\}\right) \\ &\leq P\left(|\tilde{Y}_e[M_d]| > M_d^{\alpha/2} \varepsilon^\alpha \log 1/\varepsilon^2\right) \\ &\leq P\left(|\tilde{Y}_e[M_d]| > M_d^{\alpha/2} \varepsilon^\alpha \log 1/\varepsilon^2, \mathcal{B}\right) + P(\mathcal{B}^c) \end{aligned} \quad (18)$$

279 Now under the event  $\mathcal{B}$  with (2),  $|\tilde{Y}_e[M_d]| \leq \frac{3}{2}|\tilde{K}[M_d]| \leq C|M_d|^{-\nu}$ . Further, by definition of  
280  $M_d$  and (2)

$$M_d \asymp \left(\varepsilon^\alpha (\log 1/\varepsilon)^{2/3}\right)^{-2/(2\nu+\alpha)} \quad (19)$$

281 which means that as  $n \rightarrow \infty$ ,  $M_d^{-\nu-\alpha/2} = o(\varepsilon^\alpha (\log 1/\varepsilon^2))$ . Hence, from (18) with (19) and  
282 (17), there is an  $N \in \mathbb{Z}^+$  such that for all  $n \geq N$ ,

$$P(M > M_d) \leq P(M_d^{-\nu-\alpha/2} > \varepsilon^\alpha \log 1/\varepsilon^2) + P(\mathcal{B}^c) = P(\mathcal{B}^c) = \mathcal{O}(\Omega_n). \quad (20)$$

On the other hand,

$$\begin{aligned} P(M < M_c) &\leq P\left(\bigcup_{\omega=1}^{M_c-1} \left\{ |\tilde{Y}_e[\omega]| \leq \omega^{\alpha/2} \varepsilon^\alpha \log 1/\varepsilon^2 \right\}\right) \\ &\leq \sum_{\omega=1}^{M_c-1} P\left(|\tilde{Y}_e[\omega]| \leq \omega^{\alpha/2} \varepsilon^\alpha \log 1/\varepsilon^2\right). \end{aligned}$$

283 Under the event  $\mathcal{B}$ ,  $|\tilde{Y}_e[\omega]| \geq |\tilde{K}[\omega]|/2 \geq cM_c^{-\nu}$  for all  $\omega = 1, 2, \dots, M_c - 1$ . Similar to (19),  
284 by (15) and (2),

$$M_c \asymp \left(\varepsilon^\alpha (\log 1/\varepsilon^2)^{4/3}\right)^{-2/(2\nu+\alpha)} \quad (21)$$

285 and consequently, as  $n \rightarrow \infty$ ,  $\varepsilon^\alpha(\log 1/\varepsilon^2) = o(M_c^{-\nu-\alpha/2})$ . Hence from (17),

$$P(M < M_c) \leq P(\mathcal{B}^c) = \mathcal{O}(\Omega_n). \quad (22)$$

286 Therefore, (20) with (22) yields the first result of the Lemma. The second result of the  
287 Lemma follows from (19) and (21).  $\square$

### 288 5.1. Maxiset Theorem

As in similar previous works in Kulik and Raimondo (2009a); Johnstone et al. (2004) the proof of the main result imitates the same maxiset approach. Roughly speaking, this approach finds the ‘maxiset’ class of functions for a general hard thresholding wavelet estimator. This Maxiset theorem is stated here for easy reference. First, introduce the notation:  $\mu$  will denote the measure such that for  $j \in \mathbb{N}$ ,  $k \in \mathbb{N}$ ,

$$\begin{aligned} \mu \{(j, k)\} &= \|\sigma_{j,\nu,\alpha} \Psi_{j,k}\|_p^p = \sigma_{j,\nu,\alpha}^p 2^{j(\frac{p}{2}-1)} \|\Psi\|_p^p, \\ l_{q,\infty}(m) &= \left\{ f, \sup_{\lambda>0} \lambda^q \mu \{(j, k) : |\beta_{j,k}| > \sigma_{j,\nu,\alpha} \lambda\} < \infty \right\}. \end{aligned}$$

289  
290 **Theorem 2 (Maxiset).** *Let  $p > 0$ ,  $0 < q < p$  and  $\{\Psi_{j,k}, j \geq -1, k = 0, 1, \dots, 2^{j-1}\}$  be a  
291 periodised wavelet basis of  $\mathcal{L}_2([0, 1])$  and  $\sigma_j$  is a positive sequence such that the heteroscedastic  
292 basis  $\sigma_j \Psi_{j,k}$  satisfies the Temlyakov property. Suppose that the index set  $\Lambda_n$  is a set of pairs  
293  $(j, k)$  and  $c_n$  is a deterministic sequence tending to zero with,*

$$\sup_n \mu(\Lambda_n) c_n^p < \infty. \quad (23)$$

294 *If for any  $n$  and any pair  $(j, k) \in \Lambda_n$  we have,*

$$\mathbb{E}|\widehat{\beta}_{j,k} - \beta_{j,k}|^{2p} \leq C(\sigma_j c_n)^{2p}; \quad P(|\widehat{\beta}_{j,k} - \beta_{j,k}| \geq \xi \sigma_j c_n / 2) \leq C(c_n^{2p} \wedge c_n^4) \quad (24)$$

295 *for some positive constants  $\xi$  and  $C$  then the wavelet estimator,*

$$\widehat{f}_n(x) = \sum_{(j,k) \in \Lambda_n} \widehat{\beta}_{j,k} \Psi_{j,k}(x) \mathbb{1}_{\{|\widehat{\beta}_{j,k}| \geq \xi \sigma_j c_n\}}$$

296 *satisfies the following for all positive integers  $n$ ,*

$$\mathbb{E} \left\| \widehat{f}_n - f \right\|_p^p \leq C c_n^{p-q}.$$

297 *if and only if,*

$$f \in l_{q,\infty}(\mu) \quad \text{and} \quad \sup_{n \geq 1} \left( c_n^{q-p} \left\| f - \sum_{j,k \in \Lambda_n} \beta_{j,k} \Psi_{j,k} \right\|_p^p \right) < \infty. \quad (25)$$



The proof of the rate result in [Theorem 1](#) will use the Maxiset Theorem by verifying the regularity conditions, [\(23\)](#), [\(24\)](#) and [\(25\)](#), then choosing  $q$  for the *dense* and *sparse* regions respectively with,

$$q = q_d := \frac{p(2\nu + \alpha)}{2s + 2\nu + \alpha} \quad \text{when } s \geq (\nu + \alpha/2)(p/\pi - 1) \quad (26)$$

$$q = q_s := \frac{(2\nu + \alpha)p - 2}{2s + 2\nu + \alpha - \frac{2}{\pi}} \quad \text{when } 1/\pi - \alpha/2 - \nu \leq s < (\nu + \alpha/2)(p/\pi - 1) \quad (27)$$

## 5.2. Stochastic analysis of the estimated wavelet coefficients

By definition, it is clear that the estimated wavelet coefficients have no bias. Consider now the covariance structure of the  $\widetilde{Z}_H$  process,

$$\text{Cov} \left( \widetilde{Z}_H[\omega], \widetilde{Z}_H[\ell] \right) = \mathbb{E} \widetilde{Z}_H[\omega] \overline{\widetilde{Z}_H[\ell]} = \mathbb{E} \int_{\mathbb{R}} e^{-2\pi i \omega x} dB_H(x) \int_{\mathbb{R}} e^{2\pi i \ell y} dB_H(y).$$

To evaluate this, appeal to [Theorem 2](#) of [Wang \(1996\)](#) which uses a representation of the fractional Gaussian noise process via a Wavelet-Vaguelette Decomposition (WVD)

$$dB_H(x) = \sum_{j,k} \xi_{j,k} u_{j,k}(x) dx,$$

where  $\xi_{j,k}$  is a white noise process and  $u_{j,k}$  is a set of vaguelette basis functions defined with,

$$u_{j,k}(x) := (-\Delta)^{1/4-H/2} \varphi_{j,k}(x),$$

where  $\Delta = \frac{d^2}{dx^2}$  is an elliptic operator and  $\varphi_{j,k}: \mathbb{R} \rightarrow \mathbb{R}$  is a set of orthogonal wavelet functions. Using this representation of fractional Gaussian noise we can write,

$$\begin{aligned} \text{Cov} \left( \widetilde{Z}_H[\omega], \widetilde{Z}_H[\ell] \right) &= \sum_{j,k} \sum_{j',k'} \mathbb{E} \xi_{j,k} \xi_{j',k'} \int_{\mathbb{R}} e^{-2\pi i \omega x} u_{j,k}(x) dx \int_{\mathbb{R}} e^{2\pi i \ell y} u_{j',k'}(y) dy. \\ &= \sum_{j,k} \widehat{u_{j,k}[\omega]} \overline{\widehat{u_{j,k}[\ell]}}. \end{aligned} \quad (28)$$

The operator  $(-\Delta)^{-(H-1/2)/2}$  for  $H \in (1/2, 1)$  is known from the theory of singular integrals as the *Reisz Potential* (see for example [Stein, 1970](#), Chapter V) and has the representation,

$$(-\Delta)^{-\frac{H-1/2}{2}} f(x) = \frac{\Gamma\left(\frac{3}{4} - \frac{H}{2}\right)}{\sqrt{\pi} 2^{H-\frac{1}{2}} \Gamma\left(\frac{H}{2} - \frac{1}{4}\right)} \int_{\mathbb{R}} f(z) |z-x|^{H-3/2} dz. \quad (29)$$

For our purposes its behaviour in the Fourier domain has been evaluated by [Samko, Kilbas, and Marichev \(1993\)](#). Indeed, apply [Theorem 12.2](#) of [Samko et al. \(1993\)](#) with [\(29\)](#) then for any  $f \in \mathcal{L}_1(\mathbb{R})$ ,

$$\mathcal{F}(-\Delta)^{1/4-H/2} f(\omega) = \widetilde{f}(\omega) |\omega|^{1/2-H}. \quad (30)$$

306 From (28) and (30), it would be desirable to use a wavelet function  $\varphi \in \mathcal{L}_1(\mathbb{R})$  that has a  
 307 simple behaviour in the Fourier domain. Naturally, a suitable choice is the Meyer wavelet,  
 308  $\varphi = \psi$ , since it is bandlimited (see Section 2.1) and makes the calculations easier. Therefore  
 309 we have,

$$\text{Cov} \left( \widetilde{Z}_H[\omega], \widetilde{Z}_H[\ell] \right) = |\omega\ell|^{1/2-H} \sum_{j,k} \widetilde{\psi}_{j,k}(\omega) \overline{\widetilde{\psi}_{j,k}(\ell)}. \quad (31)$$

Consider an arbitrary  $\omega \in \mathbb{Z}$  and consider the possible values of  $j$  such that  $\omega \in \mathbb{D}_j$ . The summation sets will have a non empty intersection,  $\mathbb{D}_j \cap \mathbb{D}_{j'} \neq \emptyset$ , if and only if  $j' \in \{j-1, j, j+1\}$ . Therefore the summands in (31) will be nonzero for, at most, three different values of  $j$ . The Meyer wavelet also is bounded with,  $|\widetilde{\psi}| \leq 1$ . Therefore we can crudely bound the magnitude of the covariance with,

$$\begin{aligned} \left| \text{Cov} \left( \widetilde{Z}_H[\omega], \widetilde{Z}_H[\ell] \right) \right| &= |\omega\ell|^{1/2-H} \left| \sum_{j \in \mathbb{Z}} \sum_{k=0}^{2^j-1} 2^{-j} e^{2^{1-j}\pi i(\ell-\omega)k} \widetilde{\psi}(\omega 2^{-j}) \overline{\widetilde{\psi}(\ell 2^{-j})} \right| \\ &\leq 3|\omega\ell|^{1/2-H}. \end{aligned} \quad (32)$$

Thus we are in a position to bound the variance of the estimated wavelet coefficients,

$$\begin{aligned} \text{Var} \left( \widehat{\beta}_{j,k} \right) &= \varepsilon^{2\alpha} \text{Var} \left( \sum_{\ell \in \mathbb{D}_j} \frac{\widetilde{Z}_H[\ell]}{\widetilde{K}[\ell]} \overline{\widetilde{\Psi}_{j,k}[\ell]} \right) \\ &= \varepsilon^{2\alpha} \sum_{\omega \in \mathbb{D}_j} \sum_{\ell \in \mathbb{D}_j} \frac{\overline{\widetilde{\Psi}_{j,k}[\ell]} \widetilde{\Psi}_{j,k}[\omega]}{\widetilde{K}[\ell] \widetilde{K}[\omega]} \text{Cov} \left( \widetilde{Z}_H[\omega], \widetilde{Z}_H[\ell] \right) =: \varepsilon^{2\alpha} \tau_{\alpha,j,k}^2. \end{aligned} \quad (33)$$

To gain insight to the overall asymptotic structure, the variance of the coefficients needs to be bounded. Use (32) and that the cardinality of  $\mathbb{D}_j$ ,  $|\mathbb{D}_j| = 2^{j+1}$ ,

$$\begin{aligned} \tau_{\alpha,j}^2 &\leq 3 \sum_{\omega \in \mathbb{D}_j} \left| \frac{\widetilde{\Psi}_{j,k}[\omega]}{\widetilde{K}[\omega]} \right| |\omega|^{1/2-H} \sum_{\ell \in \mathbb{D}_j} \left| \frac{\overline{\widetilde{\Psi}_{j,k}[\ell]}}{\widetilde{K}[\ell]} \right| |\ell|^{1/2-H} \\ &= 3 \left( \sum_{\omega \in \mathbb{D}_j} \left| \frac{\widetilde{\Psi}_{j,k}[\omega]}{\widetilde{K}[\omega]} \right| |\omega|^{1/2-H} \right)^2 \\ &\leq 3 |\mathbb{D}_j| 2^{-j} \sum_{\omega \in \mathbb{D}_j} \left| \frac{\widetilde{\Psi}[\omega 2^{-j}]}{\widetilde{K}[\omega]} \right|^2 |\omega|^{1-2H} \\ &\leq 6 \sum_{\omega \in \mathbb{D}_j} \left| \frac{\widetilde{\Psi}[\omega 2^{-j}]}{\widetilde{K}[\omega]} \right|^2 |\omega|^{1-2H} \\ &\leq 6 \sup_{x \in \mathbb{D}_j} |x|^{1-2H} \sup_{y \in \mathbb{D}_j} |\widetilde{K}[y]|^{-2} \int_{\mathbb{R}} |\widetilde{\Psi}(z)|^2 dz \\ &\leq C 2^{-j(1-\alpha-2\nu)} \|\Psi\|_2^2, \end{aligned}$$

310 where the last two lines follow by Parseval and Plancherels identities and condition (2).  
 311 Thus, the asymptotic behaviour of the variance of the wavelet coefficients at scale  $j$  are  
 312 bounded with,

$$\text{Var}\left(\widehat{\beta}_{j,k}\right) = \varepsilon^{2\alpha} \tau_{\alpha,j}^2 \leq C \varepsilon^{2\alpha} 2^{-j(1-\alpha-2\nu)} \leq C \sigma_{j,\nu,\alpha}^2 c_n^2,$$

313 where  $\sigma_{j,\nu,\alpha}$  and  $c_n$  are defined in (10) and (11). Since  $\widehat{\beta}_{j,k}$  is Gaussian, then from the variance  
 314 bound it follows that,

$$\mathbb{E}\left|\widehat{\beta}_{j,k} - \beta_{j,k}\right|^{2p} \leq C_p(\sigma_{j,\nu,\alpha} c_n)^{2p}.$$

Let  $\xi \geq \sqrt{4\alpha(p \vee 2)}$  and  $Z \sim \mathcal{N}(0, 1)$ , then from the tail inequality for Gaussian random variables.

$$\begin{aligned} P\left(\left|\widehat{\beta}_{j,k} - \beta_{j,k}\right| \geq \frac{\xi \tau_{j,\nu,\alpha} c_n}{2}\right) &= 2P\left(Z \geq \frac{\xi \sqrt{\log n}}{2}\right) \\ &\leq \frac{2\sqrt{2}}{\xi \sqrt{\pi \log n}} \exp\left\{-\frac{\xi^2 \log n}{4}\right\} \\ &\leq C_\xi n^{-\frac{\xi^2}{4}} \leq C(c_n^{2p} \wedge c_n^4). \end{aligned}$$

315 This verifies the wavelet coefficient conditions in (24).

### 316 5.3. Temlyakov Property and resolution tuning

317 Recall  $\Lambda_n = \{(j, k) : -1 \leq j \leq j_{\alpha,1}; k = 0, 1, \dots, 2^j - 1\}$ . Consider the set of scales  $\Lambda_n^1 =$   
 318  $\{j \in \mathbb{Z} : -1 \leq j \leq j_{\alpha,1}, j_{\alpha,1} \in \mathbb{Z}^+\}$ . Then from [Johnstone et al. \(2004, Appendices A.1 &](#)  
 319 [B.2\)](#), the heteroskedastic basis  $\{\sigma_j, \Psi_{j,k}(\cdot)\}$  satisfies the Temlyakov property as soon as,

$$\sum_{j \in \Lambda_n^1} 2^j \sigma_j^2 \leq C \sup_{j \in \Lambda_n^1} (2^j \sigma_j^2) \quad \text{and} \quad \sum_{j \in \Lambda_n^1} 2^{jp/2} \sigma_j^2 \leq C \sup_{j \in \Lambda_n^1} (2^{jp/2} \sigma_j^p).$$

This property is satisfied in our framework with  $\sigma_j = \sigma_{j,\nu,\alpha} \leq C 2^{-j/2(1-\alpha-2\nu)}$ . Now verify the resolution tuning condition (23).

$$\mu(\Lambda_n) = \sum_{j \leq j_{\alpha,1}} 2^j \sigma_{j,\nu,\alpha}^p 2^{j(p/2-1)} \|\Psi\|_p^p < C 2^{j_{\alpha,1} p(\alpha+2\nu)/2}.$$

320 Using the choice,  $2^{j_{\alpha,1}} \asymp (n^\alpha / \log n)^{1/(\alpha+2\nu)}$  yields  $\mu(\Lambda_n) c_n^p = \mathcal{O}(1)$ . Consequently, (23) is  
 321 verified.

### 322 5.4. Besov Embedding

323 One needs to find a Besov scale such that  $\mathcal{B}_{\pi,r}^\delta \subseteq l_{q,\infty}$  and that the maxiset condition (25)  
 324 holds. As shown in [Johnstone et al. \(2004\)](#), the problem can be simplified by considering

325 the the set of functions  $l_q(\mu) \subset l_{q,\infty}(\mu)$  where,

$$l_q(\mu) := \left\{ f \in \mathcal{L}_p : \sum_{j,k \in A_j} \frac{|\beta_{j,k}|^q}{\sigma_j^q} \|\sigma_j \Psi_{j,k}\|_p^p < \infty \right\},$$

326 where  $A_j$  is a set of cardinality proportional to  $2^j$ . Since  $\|\sigma_j \Psi_{j,k}\|_p^p = \sigma_j^p 2^{j(\frac{p}{2}-1)}$ , then  $f \in l_q(\mu)$

327 if

$$\sum_{j \geq 0} 2^{\frac{j}{2}(p-2-(p-q)(1-\alpha-2\nu))} \sum_{k=0}^{2^j-1} |\beta_{j,k}|^q = \sum_{j \geq 0} 2^{jq\left((\nu+\frac{\alpha}{2})\left(\frac{p}{q}-1\right)+\frac{1}{2}-\frac{1}{q}\right)} \sum_{k=0}^{2^j-1} |\beta_{j,k}|^q < \infty.$$

This condition is true for  $f \in \mathcal{B}_{q,q}^\delta$  with the choice  $\delta = (\nu + \frac{\alpha}{2})(\frac{p}{q} - 1)$ . Then depending on whether we are in the dense or sparse case the levels  $s, \pi$  and  $r$  are determined such that  $\mathcal{B}_{\pi,r}^s \subseteq \mathcal{B}_{q,q}^\delta$ . There exists two Besov embeddings given by,

$$\mathcal{B}_{\pi,r}^s \subseteq \mathcal{B}_{\rho,r}^\gamma \quad \text{when } 0 < \rho \leq \pi \text{ and } s \geq \gamma; \quad (34)$$

$$\mathcal{B}_{\pi,r}^s \subseteq \mathcal{B}_{\rho,r}^\gamma \quad \text{when } \pi < \rho \text{ and } s - 1/\pi = \gamma - 1/\rho. \quad (35)$$

328 **The dense phase.** Choose the level of  $q = q_d$  where,

$$q_d := \frac{p(2\nu + \alpha)}{2s + 2\nu + \alpha} \quad \text{when } s \geq (\nu + \alpha/2)(p/\pi - 1).$$

329 Then find the levels  $s, \pi$  and  $r$  such that  $\mathcal{B}_{\pi,r}^s \subseteq \mathcal{B}_{q_d,q_d}^\delta$  where  $s \geq (\nu + \alpha/2)(p/\pi - 1)$ .

330 By definition, one has,  $s \geq (\alpha/2 + \nu)(p/\pi - 1)$ . Eliminate  $p$  by substituting  $p = (2s +$   
 331  $2\nu + \alpha)q_d/(2\nu + \alpha)$  yields,  $\pi \geq q_d$ . So we need to prove  $s \geq \delta = (2\nu + \alpha)(p/2q_d - 1/2)$  to  
 332 be able to use (34). However, by definition of  $q_d$  we have,  $\delta = (\nu + \alpha/2)(p/q_d - 1) = s > 0$   
 333 by assumption.

334 **The sparse phase.** Choose the level of  $q = q_s$  where,

$$q_s := \frac{(2\nu + \alpha)p - 2}{2s + 2\nu + \alpha - \frac{2}{\pi}} \quad \text{when } 1/\pi - \alpha/2 - \nu < s < (\nu + \alpha/2)(p/\pi - 1).$$

To ensure the inequalities in the above equation are valid, it requires that  $p > 2/(2\nu + \alpha)$ .

Then  $\delta = (2\nu + \alpha)(p/2q_s - 1/2)$  and we have,

$$\begin{aligned} \delta &= (2\nu + \alpha)(p/2q_s - 1/2) \\ &= \frac{(2\nu + \alpha)(sp - p/\pi + 1)}{(2\nu + \alpha)p - 2}. \end{aligned}$$

335 Consider the scenario when  $\pi \geq q_s$  and use embedding (34). This requires that  $s \geq \delta =$   
 336  $(2\nu + \alpha)(sp - p/\pi + 1)/((2\nu + \alpha)p - 2)$ , or equivalently,  $s \leq (\nu + \alpha/2)(p/\pi - 1)$ . It is also  
 337 needed that  $\delta > 0$ , which implies that either (i)  $p > 2/(2\nu + \alpha)$  and  $s > 1/\pi - 1/p$ ; or (ii)

338  $p < 2/(2\nu + \alpha)$  and  $s < 1/\pi - 1/p$ . The (ii) scenario is impossible since it is assumed that  
 339  $p \geq 1$  and  $s \geq 1/\pi$  which contradicts  $s < 1/\pi - 1/p$ . The condition  $p > 2/(2\nu + \alpha)$  is verified  
 340 since by assumption in the sparse phase,  $\nu \geq 1 - \alpha/2$  and  $p > 1$ . Then (i) implies that,  
 341  $s \geq 1/\pi - \nu - \alpha/2$ .

342 Consider now the scenario when  $\pi < q_s$  by defining,

$$s' = s - 1/\pi + 1/q. \quad (36)$$

343 Then use the embedding (35). Indeed, if we solve (36) with  $s' = \delta$ , then  $q = q_s$  and the  
 344 embedding of (35) applies.

To apply Theorem 2, (25) needs to be verified. Therefore we need to find a  $\delta > 0$  such that for any  $f \in \mathcal{B}_{p,r}^\delta$ , (25) is satisfied.

$$c_n^{q-p} \left\| f - \sum_{j,k} \beta_{j,k} \Psi_{j,k} \right\|_p^p = c_n^{q-p} 2^{-j_{\alpha,1} \delta p} \|f\|_{\mathcal{B}_{p,r}^\delta}^p = c_n^{q-p+2\delta p/(2\nu+\alpha)} \|f\|_{\mathcal{B}_{p,r}^\delta}^p.$$

345 The above is bounded uniformly in  $n$  if we choose  $\delta = 1/2(2\nu + \alpha)(1 - q/p)$ . Now we need  
 346 to find  $s, \pi$  such that  $\mathcal{B}_{\pi,r}^s \subseteq \mathcal{B}_{p,r}^\delta$ .

Consider the first case  $\pi \geq p$ . This case cannot occur in the sparse phase due to (13) and the assumption that  $s$  is positive. In the dense phase, use embedding (34) with  $\gamma = \delta$  and  $q = q_d$ . Therefore, (34) holds if  $s \geq 1/2(2\nu + \alpha)(1 - q_d/p)$ . This implies,

$$\begin{aligned} s &\geq 1/2(2\nu + \alpha)(1 - q_d/p) \\ &= \frac{(2\nu + \alpha)s}{2s + 2\nu + \alpha}, \end{aligned}$$

347 which always holds under the assumption that  $s > 0$ .

348 Now consider the dense case when  $\pi < p$ . In this scenario use embedding (35) by defining  
 349  $s - 1/\pi = \gamma - 1/p$  which ensures  $\mathcal{B}_{\pi,r}^s \subseteq \mathcal{B}_{p,r}^\gamma$ . Then complete the embedding using (34)  
 350 (namely,  $\mathcal{B}_{p,r}^\gamma \subseteq \mathcal{B}_{p,r}^\delta$ ) which requires  $\gamma \geq \delta$  with  $q = q_d$  or equivalently after rearrangement,  
 351  $2s\gamma + (2\nu + \alpha)(1/p - 1/\pi) \geq 0$ . The left hand side is greater than  $(s - 1/\pi)(p/\pi - 1)(2\nu + \alpha) \geq 0$   
 352 when  $s \geq (\nu + \alpha/2)(p/\pi - 1)$  (which is true in the dense phase).

353 The last case to consider is the sparse case when  $\pi < p$ . Again introduce a new Besov  
 354 scale  $\gamma$  defined with,  $s - 1/\pi = \gamma - 1/p$  and apply a similar argument to above which requires  
 355 that,  $\gamma \geq \delta$  with  $q = q_s$ . This is satisfied if  $s > 1/\pi$ , which always holds.

### 356 5.5. Proof of Theorem 1

357 The proof of the theorem is an application of Theorem 2 with the choice of  $\sigma_j = \sigma_{j,\nu,\alpha}$  and  
 358  $c_n$  and  $\xi$  defined in Section 3.1 and the arguments in Section 5.2, Section 5.3 and Section 5.4.

359 The dense regime rate result of (12) is derived with the choice of  $q = q_d$  in (26) and the Besov  
360 embedding argument in Section 5.4. Similarly, the sparse rate regime in (13) is derived with  
361 the Besov embedding result in Section 5.4 with the choice of  $q = q_s$  in (27).

## 362 Acknowledgements

363 I would like to acknowledge The University of Sydney since part of this work was achieved  
364 there. I would also like to thank Rafał Kulik for helpful comments. This research was  
365 partially supported under Australian Research Council's Discovery Projects funding scheme  
366 (project number DP110100670).

## 367 References

368 Abramovich, F., Silverman, B. W., 1998. Wavelet decomposition approaches to statistical  
369 inverse problems. *Biometrika* 85 (1), 115–129.

370 URL <http://dx.doi.org/10.1093/biomet/85.1.115>

371 Beran, J., 1992. Statistical Methods for Data with Long-Range Dependence. *Statistical Sci-*  
372 *ence* 7 (4), 404–416.

373 URL <http://dx.doi.org/10.1214/ss/1177011127>

374 Beran, J., 1994. Statistics for long-memory processes. Vol. 61 of *Monographs on Statistics*  
375 *and Applied Probability*. Chapman and Hall, New York.

376 Cavalier, L., Raimondo, M., 2007. Wavelet deconvolution with noisy eigenvalues. *IEEE*  
377 *Trans. Signal Process.* 55 (6, part 1), 2414–2424.

378 URL <http://dx.doi.org/10.1109/TSP.2007.893754>

379 Chesneau, C., 2012. On the adaptive wavelet deconvolution of a density for strong mixing  
380 sequences. *J. Korean Statist. Soc.*

381 URL <http://dx.doi.org/10.1016/j.jkss.2012.01.005>

382 Donoho, D., Johnstone, I., Kerkycharian, G., Picard, D., 1995. Wavelet Shrinkage - Asymp-  
383 *topia*. *Journal of the Royal Statistical Society Series B-Methodological* 57 (2), 301–337.

384 Donoho, D. L., 1995. Nonlinear solution of linear inverse problems by wavelet-vaguelette  
385 decomposition. *Appl. Comput. Harmon. Anal.* 2 (2), 101–126.

386 URL <http://dx.doi.org/10.1006/acha.1995.1008>

- 387 Donoho, D. L., Johnstone, I. M., 1998. Minimax estimation via wavelet shrinkage. *Ann.*  
388 *Statist.* 26 (3), 879–921.  
389 URL <http://dx.doi.org/10.1214/aos/1024691081>
- 390 Donoho, D. L., Raimondo, M. E., 2004. Translation invariant deconvolution in a periodic  
391 setting. *Int. J. Wavelets Multiresolut. Inf. Process.* 2 (4), 415–431.
- 392 Doukhan, P., Oppenheim, G., Taqqu, M. S. (Eds.), 2003. *Theory and applications of long-*  
393 *range dependence.* Birkhäuser Boston Inc., Boston, MA.
- 394 Fan, J., Koo, J.-Y., 2002. Wavelet deconvolution. *IEEE Trans. Inform. Theory* 48 (3), 734–  
395 747.  
396 URL <http://dx.doi.org/10.1109/18.986021>
- 397 Johnstone, I. M., Kerkycharian, G., Picard, D., Raimondo, M., 2004. Wavelet deconvolution  
398 in a periodic setting. *J. R. Stat. Soc. Ser. B Stat. Methodol.* 66 (3), 547–573.  
399 URL <http://dx.doi.org/10.1111/j.1467-9868.2004.02056.x>
- 400 Johnstone, I. M., Raimondo, M., 2004. Periodic boxcar deconvolution and Diophantine ap-  
401 proximation. *Ann. Statist.* 32 (5), 1781–1804.
- 402 Kalifa, J., Mallat, S., 2003. Thresholding estimators for linear inverse problems and decon-  
403 volutions. *Ann. Statist.* 31 (1), 58–109.  
404 URL <http://dx.doi.org/10.1214/aos/1046294458>
- 405 Kulik, R., 2008. Nonparametric deconvolution problem for dependent sequences. *Electron.*  
406 *J. Stat.* 2, 722–740.  
407 URL <http://dx.doi.org/10.1214/07-EJS154>
- 408 Kulik, R., Raimondo, M., 2009a.  $L^p$ -wavelet regression with correlated errors and inverse  
409 problems. *Statist. Sinica* 19 (4), 1479–1489.
- 410 Kulik, R., Raimondo, M., 2009b. Wavelet regression in random design with heteroscedastic  
411 dependent errors. *Ann. Statist.* 37 (6A), 3396–3430.  
412 URL <http://dx.doi.org/10.1214/09-AOS684>
- 413 Mallat, S., 1999. *A wavelet tour of signal processing.* Academic Press Inc., San Diego, CA.

- 414 Meyer, Y., 1992. Wavelets and operators. Vol. 37 of Cambridge Studies in Advanced Mathe-  
415 matics. Cambridge University Press, Cambridge, translated from the 1990 French original  
416 by D. H. Salinger.
- 417 Park, J., Park, C., 2009. Robust estimation of the Hurst parameter and selection of an onset  
418 scaling. *Statist. Sinica* 19 (4), 1531–1555.
- 419 Pensky, M., Sapatinas, T., 2009. Functional deconvolution in a periodic setting: uniform  
420 case. *Ann. Statist.* 37 (1), 73–104.  
421 URL <http://dx.doi.org/10.1214/07-AOS552>
- 422 Raimondo, M., Stewart, M., 7 2007. The waved transform in r: Performs fast translation-  
423 invariant wavelet deconvolution. *Journal of Statistical Software* 21 (2), 1–28.  
424 URL <http://www.jstatsoft.org/v21/i02>
- 425 Samko, S. G., Kilbas, A. A., Marichev, O. I., 1993. Fractional integrals and derivatives.  
426 Gordon and Breach Science Publishers, Yverdon, theory and applications, Edited and  
427 with a foreword by S. M. Nikol'skiĭ, Translated from the 1987 Russian original, Revised  
428 by the authors.
- 429 Stein, E. M., 1970. Singular integrals and differentiability properties of functions. Princeton  
430 Mathematical Series, No. 30. Princeton University Press, Princeton, N.J.
- 431 Veitch, D., Abry, P., 1999. A wavelet-based joint estimator of the parameters of long-range  
432 dependence. *IEEE Trans. Inform. Theory* 45 (3), 878–897.  
433 URL <http://dx.doi.org/10.1109/18.761330>
- 434 Walter, G. G., Shen, X., 1999. Deconvolution using Meyer wavelets. *J. Integral Equations*  
435 *Appl.* 11 (4), 515–534.  
436 URL <http://dx.doi.org/10.1216/jiea/1181074297>
- 437 Wang, Y., 1996. Function estimation via wavelet shrinkage for long-memory data. *Ann.*  
438 *Statist.* 24 (2), 466–484.  
439 URL <http://dx.doi.org/10.1214/aos/1032894449>
- 440 Wang, Y., 1997. Minimax estimation via wavelets for indirect long-memory data. *J. Statist.*  
441 *Plann. Inference* 64 (1), 45–55.  
442 URL [http://dx.doi.org/10.1016/S0378-3758\(96\)00205-4](http://dx.doi.org/10.1016/S0378-3758(96)00205-4)



$DIP = 0.7$		$\alpha$				
Signal	Method	1	0.8	0.6	0.4	0.2
Cusp	i.i.d.	0.0056 (3)	<b>0.0089</b> (3)	0.0557 (4)	0.2525 (4)	0.6633 (4)
10dB	$\xi = \sqrt{\alpha}$	<b>0.0056</b> (3)	0.0091 (3)	0.0238 (3)	0.0728 (3)	0.2235 (3)
	$\xi = \sqrt{2\alpha}$	0.0056 (3)	0.0091 (3)	<b>0.0223</b> (3)	<b>0.0606</b> (3)	<b>0.1895</b> (3)
Cusp	i.i.d.	0.0035 (5)	0.0039 (5)	0.0148 (5)	0.0650 (5)	0.1683 (5)
20dB	$\xi = \sqrt{\alpha}$	<b>0.0030</b> (5)	<b>0.0037</b> (4)	0.0070 (4)	0.0099 (3)	0.0243 (3)
	$\xi = \sqrt{2\alpha}$	0.0039 (5)	0.0042 (4)	<b>0.0054</b> (4)	<b>0.0084</b> (3)	<b>0.0206</b> (3)
Cusp	i.i.d.	0.0013 (6)	0.0014 (6)	0.0036 (6)	0.0148 (6)	0.0392 (6)
30dB	$\xi = \sqrt{\alpha}$	<b>0.0011</b> (6)	<b>0.0014</b> (5)	0.0025 (5)	0.0059 (5)	0.0069 (4)
	$\xi = \sqrt{2\alpha}$	0.0015 (6)	0.0016 (5)	<b>0.0020</b> (5)	<b>0.0034</b> (5)	<b>0.0055</b> (4)
LIDAR	i.i.d.	0.0430 (4)	0.0418 (4)	0.0517 (4)	0.0972 (4)	0.4365 (5)
10dB	$\xi = \sqrt{\alpha}$	<b>0.0363</b> (4)	<b>0.0403</b> (4)	<b>0.0512</b> (3)	0.0636 (3)	0.0993 (3)
	$\xi = \sqrt{2\alpha}$	0.0473 (4)	0.0488 (4)	0.0548 (3)	<b>0.0633</b> (3)	<b>0.0913</b> (3)
LIDAR	i.i.d.	0.0128 (5)	0.0133 (5)	<b>0.0167</b> (5)	0.0483 (6)	0.1100 (6)
20dB	$\xi = \sqrt{\alpha}$	<b>0.0103</b> (5)	<b>0.0122</b> (5)	0.0248 (4)	<b>0.0299</b> (4)	0.0393 (4)
	$\xi = \sqrt{2\alpha}$	0.0151 (5)	0.0164 (5)	0.0262 (4)	0.0305 (4)	<b>0.0382</b> (4)
LIDAR	i.i.d.	0.0049 (6)	0.0049 (7)	0.0060 (7)	0.0111 (7)	0.0230 (7)
30dB	$\xi = \sqrt{\alpha}$	<b>0.0041</b> (6)	<b>0.0044</b> (6)	<b>0.0057</b> (6)	0.0088 (6)	0.0103 (5)
	$\xi = \sqrt{2\alpha}$	0.0053 (6)	0.0054 (6)	0.0059 (6)	<b>0.0073</b> (6)	<b>0.0096</b> (5)

Table 1: MSE for the Bumps and Cusp signals with  $n = 4096$  and  $M = 1024$ , the smoothing parameter for the LRD WaveD method is  $\xi = \sqrt{\alpha}$ , the i.i.d. method uses the default  $\eta = \sqrt{6}$ . The typical estimated fine scale levels are shown in parentheses for each case.

$DIP = 0.7$		$\alpha$				
Signal	Method	1	0.8	0.6	0.4	0.2
Bumps	i.i.d.	0.7657 (4)	0.7717 (4)	<b>0.7904</b> (4)	<b>0.8277</b> (4)	<b>0.9475</b> (5)
10dB	$\xi = \sqrt{\alpha}$	<b>0.7615</b> (4)	<b>0.7705</b> (4)	0.9376 (3)	0.9511 (3)	0.9831 (3)
	$\xi = \sqrt{2\alpha}$	0.7687 (4)	0.7768 (4)	0.9380 (3)	0.9517 (3)	0.9818 (3)
Bumps	i.i.d.	0.5384 (5)	<b>0.5405</b> (5)	<b>0.2905</b> (6)	<b>0.2702</b> (6)	<b>0.3165</b> (6)
20dB	$\xi = \sqrt{\alpha}$	<b>0.5374</b> (5)	0.5405 (5)	0.5469 (5)	0.7583 (4)	0.7661 (4)
	$\xi = \sqrt{2\alpha}$	0.5391 (5)	0.5417 (5)	0.5473 (5)	0.7583 (4)	0.7660 (4)
Bumps	i.i.d.	0.0793 (7)	<b>0.0807</b> (7)	<b>0.0838</b> (7)	<b>0.0897</b> (7)	<b>0.0988</b> (7)
30dB	$\xi = \sqrt{\alpha}$	<b>0.0777</b> (7)	0.2074 (6)	0.2093 (6)	0.21246(6)	0.3141 (6)
	$\xi = \sqrt{2\alpha}$	0.0811 (7)	0.2080 (6)	0.2094 (6)	0.2118 (6)	0.3133 (6)
Doppler	i.i.d.	0.0278 (5)	<b>0.0293</b> (5)	<b>0.0369</b> (5)	<b>0.0631</b> (5)	0.1199 (5)
10dB	$\xi = \sqrt{\alpha}$	<b>0.0263</b> (5)	0.0472 (4)	0.0570 (4)	0.0689 (4)	0.1203 (3)
	$\xi = \sqrt{2\alpha}$	0.0292 (5)	0.0481 (4)	0.0568 (4)	0.0666 (4)	<b>0.1196</b> (3)
Doppler	i.i.d.	0.0103 (6)	0.0106 (6)	<b>0.0122</b> (6)	<b>0.0183</b> (6)	0.0455 (7)
20dB	$\xi = \sqrt{\alpha}$	<b>0.0096</b> (6)	<b>0.0104</b> (6)	0.0200 (5)	0.0257 (5)	0.0304 (5)
	$\xi = \sqrt{2\alpha}$	0.0107 (6)	0.0110 (6)	0.0197 (5)	0.0248 (5)	<b>0.0284</b> (5)
Doppler	i.i.d.	0.0029 (7)	0.0030 (7)	<b>0.0032</b> (7)	0.0043 (8)	0.0075 (8)
30dB	$\xi = \sqrt{\alpha}$	<b>0.0027</b> (7)	<b>0.0029</b> (7)	0.0036 (7)	0.0055 (7)	0.0094 (7)
	$\xi = \sqrt{2\alpha}$	0.0031 (7)	0.0031 (7)	0.0033 (7)	<b>0.0039</b> (7)	<b>0.0066</b> (7)

Table 2: MSE for the Doppler and LIDAR signals with  $n = 4096$  and  $M = 1024$ , the smoothing parameter for the LRD WaveD method is  $\xi = \sqrt{\alpha}$ , the i.i.d. method uses the default  $\eta = \sqrt{6}$ . The typical estimated fine scale levels are shown in parentheses for each case.